Electronic Supplementary Material (ESI) for Materials Horizons.

Self-healing, stretchable and recyclable polyurethane-PEDOT:PSS conductive blends

Jinsil Kim, Jiaxin Fan, Gayaneh Petrossian, Xin Zhou, Pierre Kateb, Noemy Gagnon-Lafrenais and Fabio Cicoira*

Department of Chemical Engineering, Polytechnique Montréal, Montréal, QC H3C 3A7, Canada

*Corresponding author. E-mail: fabio.cicoira@polymtl.ca

(a)

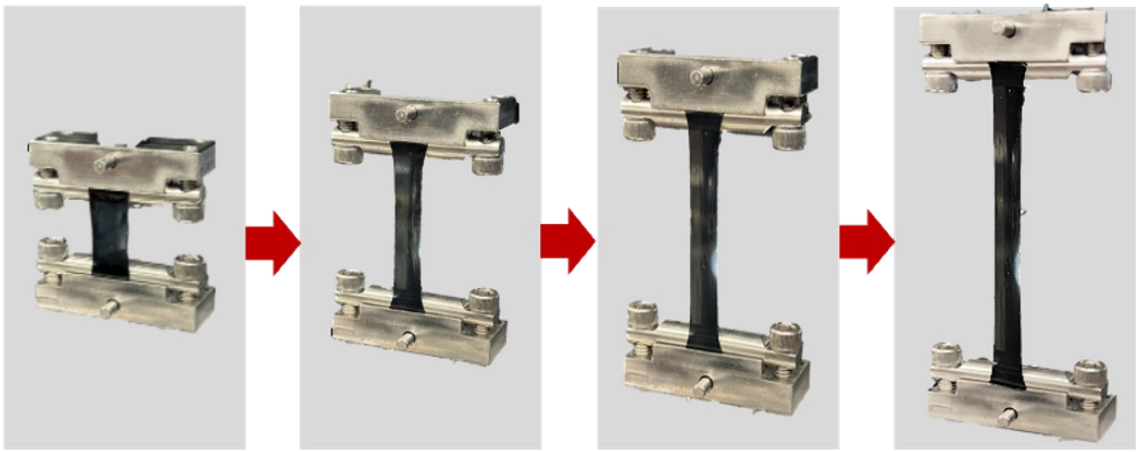

(b)

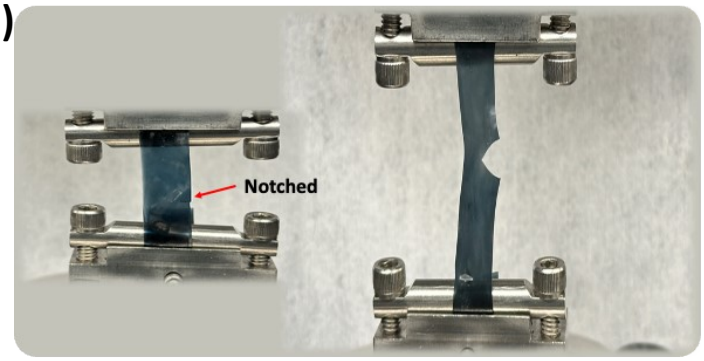

(c)

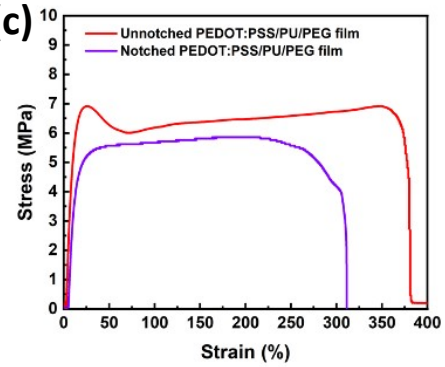

(d)

Samples	Toughness (MJ/m^3)
Unnotched PEDOT:PSS/PU/PEG film	24.60 ± 0.23
Notched PEDOT:PSS/PU/PEG film	16.54 ± 1.24

Figure S1. Photographs of a (a) PEDOT:PSS/PU/PEG film, (b) notched PEDOT:PSS/PU/PEG film under uniaxial strain and (c) tensile stress-strain curves of the unnotched and notched PEDOT:PSS/PU/PEG films. (d) Toughness of unnotched and notched PEDOT:PSS/PU/PEG film. All data (n = 3) are reported as the mean ± standard deviation.

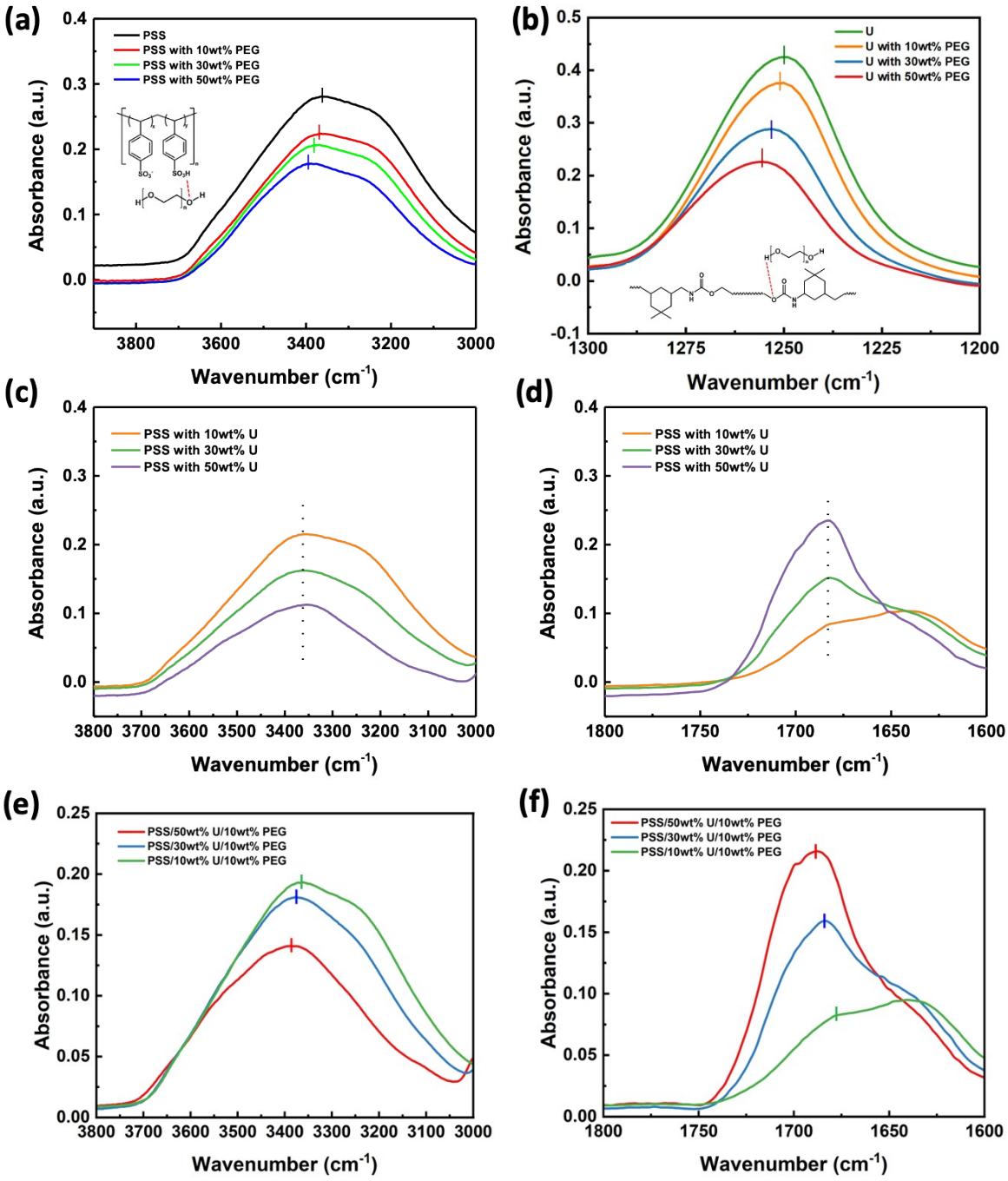

Figure S2. FTIR spectra of (a) pristine PSS and mixture of PSS/PEG with different percentages (10%, 30%, 50%). (b) pristine urethane (U) and U/PEG with different percentages (10%, 30%, 50%). (c), (d) PSS/U with different percentages (10%, 30%, 50%). (e), (f) PSS/U/PEG with different percentages (10%, 30%, 50%) of U and a fixed 10% of PEG.

Table S1.The FTIR peaks of SO_3-H and S=O bands in PSS and C-O-C and C=O bands in U.

Samples	SO_3-H in PSS (cm^{-1})	S=O in PSS (cm^{-1})	C-O-C in U (cm^{-1})	C=O in U (cm^{-1})
PSS	3360.1	1172.8	-	-
PSS/10wt% PEG	3369.4	1176.8	-	-
PSS/30wt% PEG	3381.1	1180.4	-	-
PSS/50wt% PEG	3394.6	1186.0	-	-
U	-	-	1250.1	1690.0
U/10wt% PEG	-	-	1251.3	1692.1
U/30wt% PEG	-	-	1253.2	1695.0
U/50wt% PEG	-	-	1255.8	1697.6
PSS/10wt% U				
PSS/30wt% U	3362.6	-	-	1683.3
PSS/50wt% U				
PSS/10wt% U/10wt% PEG	3366.6	-	-	1678.3
PSS/30wt% U/10wt% PEG	3376.8	-	-	1683.9
PSS/50wt% U/10wt% PEG	3381.4	-	-	1688.0

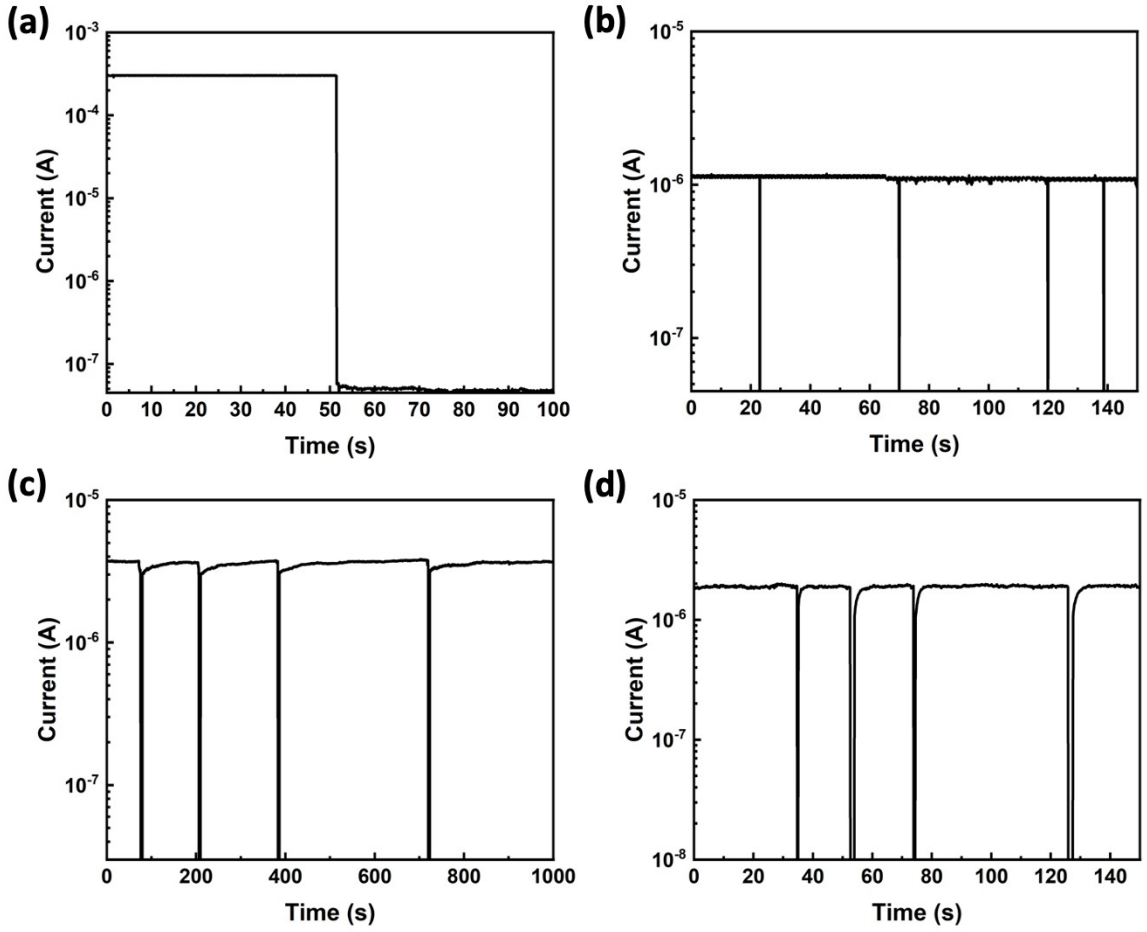

Figure S3. Current vs. time plot for (a) PEDOT:PSS, (b) PEDOT:PSS/PU, (c) PEDOT:PSS/PU/Glycerol, and (d) PEDOT:PSS/PEG/Glycerol films during several cut/healing processes.

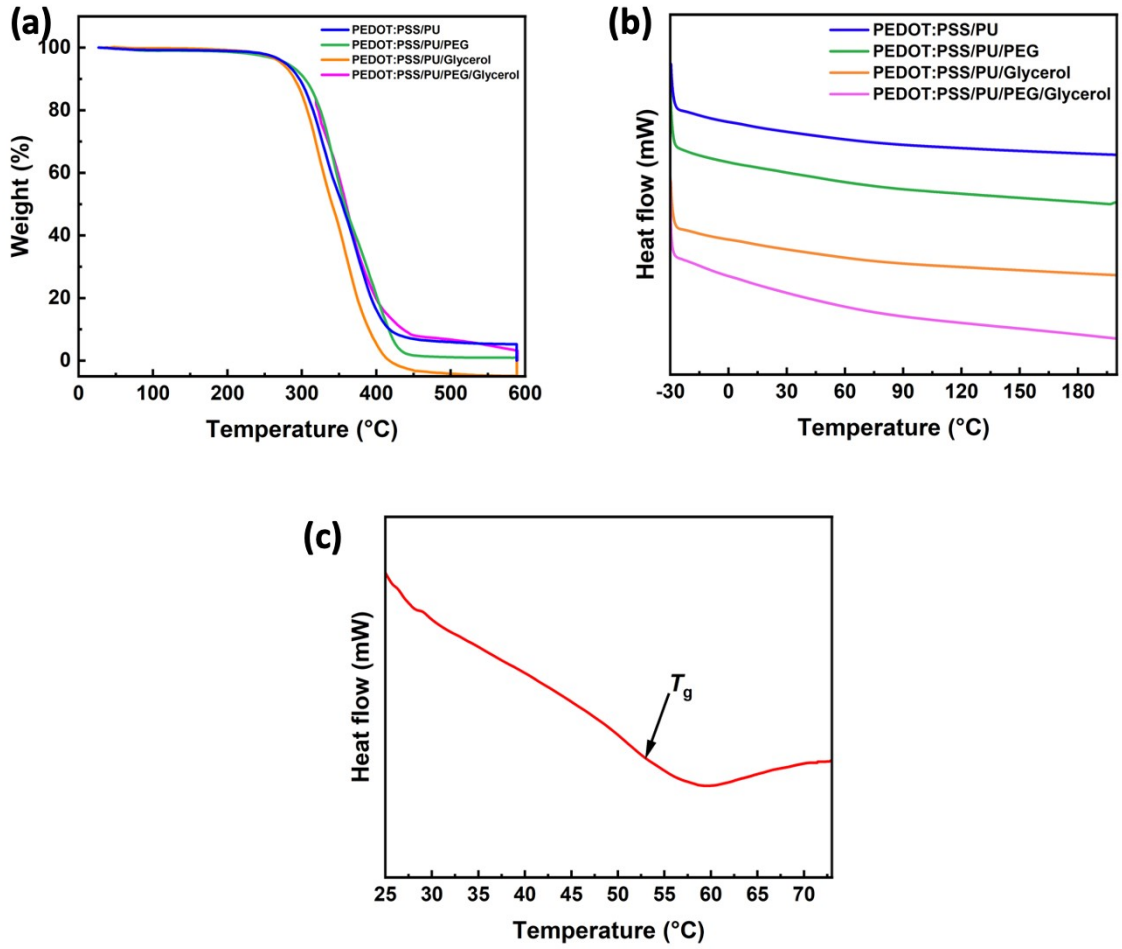

Figure S4. (a) TGA and (b) DSC thermograms of PEDOT:PSS/PU (blue), PEDOT:PSS/PU/PEG (green), PEDOT:PSS/PU/Glycerol (orange), and PEDOT:PSS/PU/PEG/Glycerol (magenta) films. (c) DSC in modulated mode thermograms of PU with glass transition temperature (T_g) at ~53 °C.

We investigated the mechanical self-healing properties of PEDOT:PSS/PU/Glycerol and PEDOT:PSS/PU/PEG/Glycerol. Notably, the PEDOT:PSS/PU/PEG/Glycerol film exhibited partial scratch recovery **(Fig. S5d)**, while the PEDOT:PSS/PU/Glycerol film ruptured under a 5N applied force **(Fig. S5c)** and showed no recovery under a 3N force scratch **(Fig. S5e)**. A healing efficiency of 55% was obtained for PEDOT:PSS/PU/PEG/Glycerol films **(Fig. S6b)**. The branched molecular structure of glycerol is identified as a potential cause for the observed decline in both the self-healing and mechanical properties, acting as a plasticizer and disrupting hydrogen bonding in the linearly structured PEG, PU, and PEDOT:PSS in the polymeric blends.

For the cut-stick self-healing tests, tensile stress-strain curves obtained from intact and healed PEDOT:PSS/PU/PEG/Glycerol demonstrated similar recovery in stretchability (**Fig. S8a**) and slightly reduced healing efficiency (**Fig. S8b**).

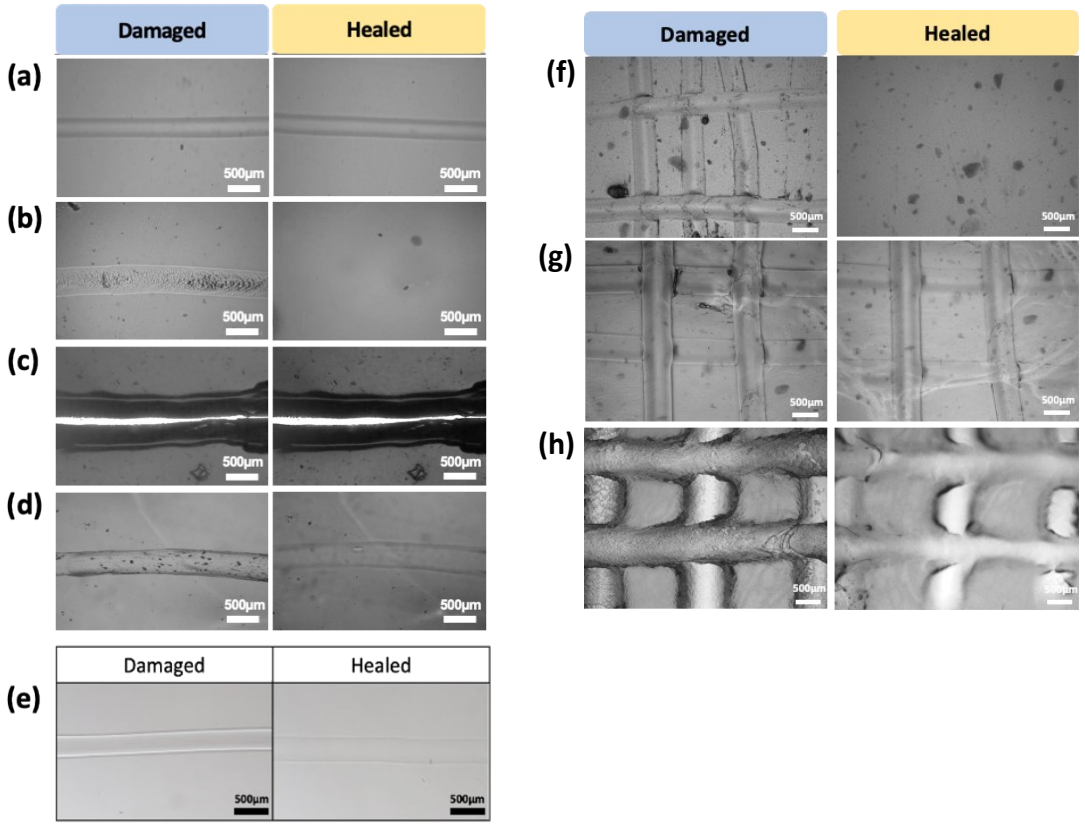

Figure S5. Optical microscope images of (a) PEDOT:PSS, (b) PEDOT:PSS/PU, (c) PEDOT:PSS/PU/Glycerol, and (d) PEDOT:PSS/PU/PEG/Glycerol after single scratching with a 5N force on the surface and healing for 10 min at 50 °C. (e) PEDOT:PSS/PU/PEG/Glycerol after surface scratching (3N) and healing for 10 min at 50 °C. (f) PEDOT:PSS/PU, (g) PEDOT:PSS/PU/Glycerol, and (h) PEDOT:PSS/PU/PEG/Glycerol after grid scratching and healing for 10 min at 50 °C.

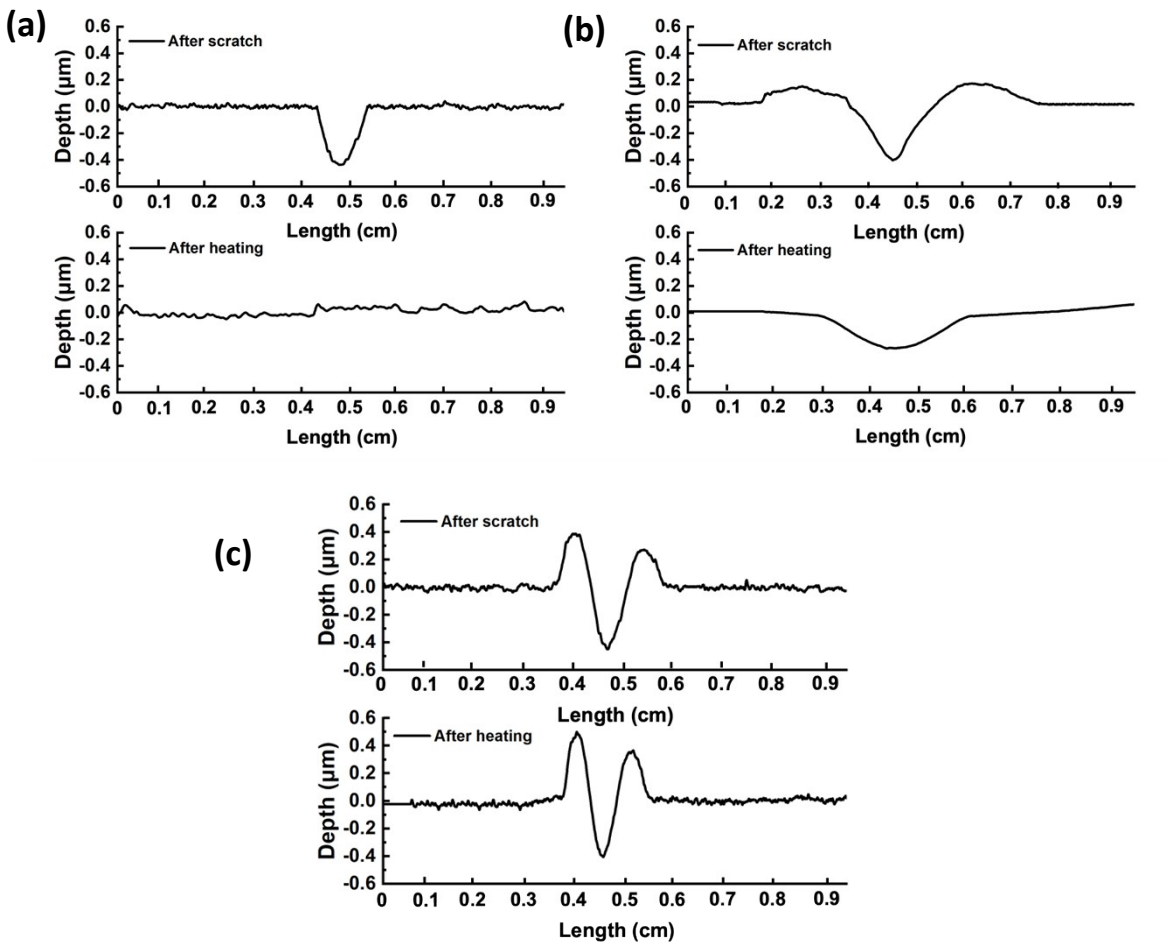

Figure S6. Depth profile for (a) PEDOT:PSS/PU, (b) PEDOT:PSS/PU/PEG/Glycerol and (c) PEDOT:PSS films scratched with 5N and healed at 50 °C for 10 min.

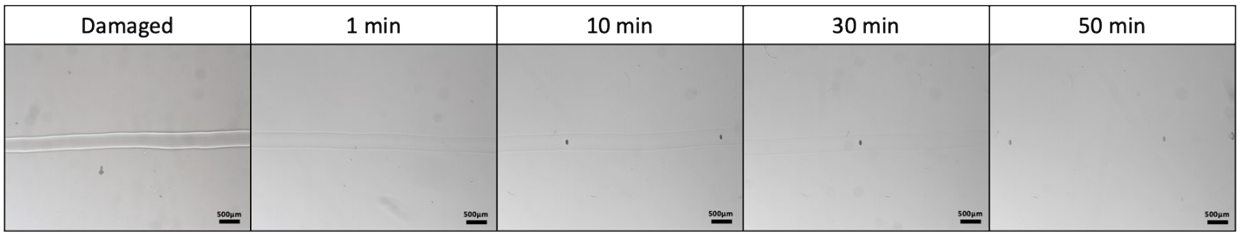

Figure S7. Optical microscope images of self-healing PU with surface scratched by 5N force and after healing for 50 min at 60 °C. The average thickness of the film was ~21 μm.

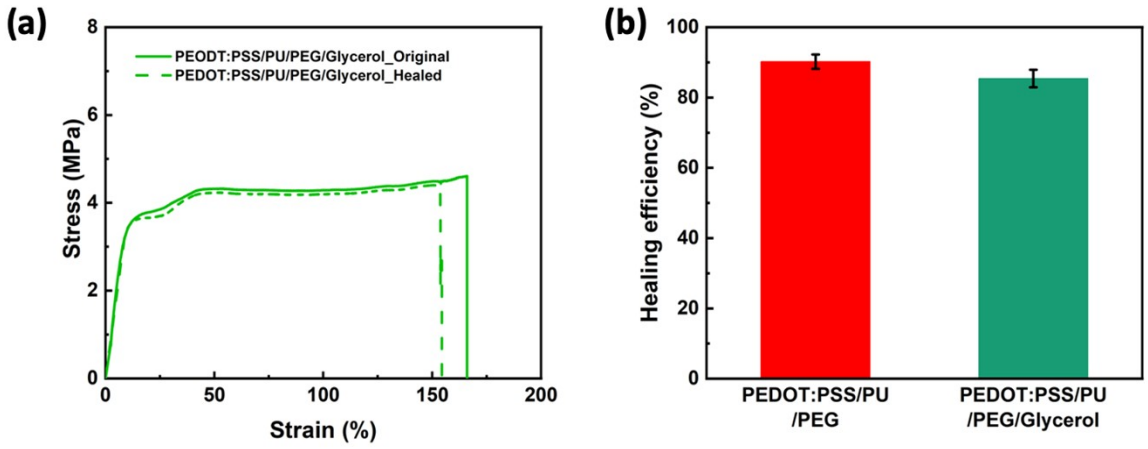

Figure S8. (a) Stress-strain curve of original and healed PEDOT:PSS/PU/PEG/Glycerol films. (b) Average healing efficiencies of PEDOT:PSS/PU/PEG and PEDOT:PSS/PU/PEG/Glycerol samples extracted from stress-strain measurements. Data for healing efficiency (n = 3) are recorded as mean ± standard deviation.

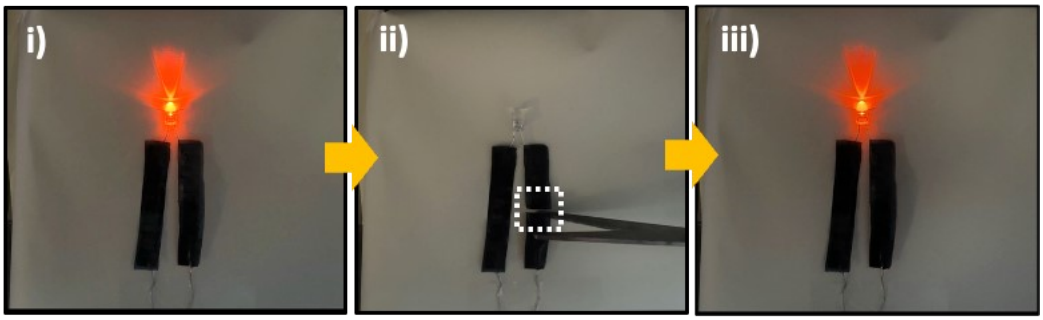

Figure S9. Demonstration of the cut and healing effect on a PEDOT:PSS/PU/PEG film connected in a circuit with an LED bulb: (i) Original, (ii) after cut and (iii) after heating at 50 °C. The sample under a constant voltage of 0.2 V.

Table S2. Summary of PEDOT:PSS-based films showing recyclable, healing behavior, maximum elongation at break, toughness, mechanical healing efficiency, conductivity, and electrical healing efficiency.

Materials	Recyclable	Healing behavior	Maximum elongation at break (%)	Toughness (MJ/m^3)	Mechanical healing efficiency (%)	Conductivity (S/cm)	Electrical healing efficiency (%)	Healing response time	Ref.
PEDOT:PSS/PEG	No	Autonomous	6.5	-	-	201	≈ 100	≈ 50–800ms	1
PEDOT:PSS/Triton X-100	No	Autonomous	57	-	-	78	≈ 70-100	≈ 1s	2
PEDOT:PSS/Glycerol	No	Water-enabled	12	-	-	500	≈ 100	≈150ms	3
PEDOT:PSS-*b*-PPEGMEA	No	Water-enabled	128	3.4	-	0.05	≈ 50	≈ 1s	4
PEDOT:PSS/PAAMPAS/IL	No	Autonomous	600	-	≈ 85	320	≈ 100	≈ 19ms	5
		Cut-stick						≈ 24h	
PANI/PAA	No	Cut-stick	470	-	≈ 99	0.1	≈ 99	≈ 24h	6
PEDOT:Tos	No	Water-enabled	-	-	-	1600	≈ 95	0.3s	7
PAAMPSA/PANI/PA	No	Autonomous	2000	-	≈ 50	200	≈ 98.6	3h	8
		Cut-stick (Pressure)							
BCOE/PEGMMA@Li/LFP	No	Cut-stick	600	-	-	1.9×10^{-4}	≈ 100	1h	9
Poly(PDES)-PA	No	Cut-stick	1300	-	≈ 91.5	7.8×10^{-4}	≈ 100	48h	10
PEDOT:PSS/PU/PEG	Yes	Autonomous	350	24.6	≈ 90	15.4	≈ 100	≈ 0.1s	This work
		Cut-stick (heated at 50 °C)						≈ 5min	

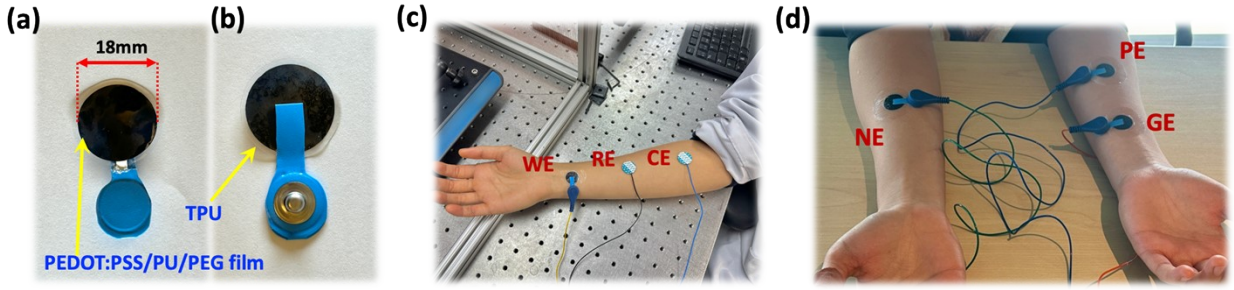

Figure S10. Photographs showing the (a) front and (b) back view of the electrodes. (c) Photograph of the skin-electrode impedance and ECG measurement configuration. The PEDOT:PSS/PU/PEG film acted as the working electrode (WE), and commercial Ag/AgCl gel disk electrodes (Natus®) were used as the reference (RE) and counter (CE) electrodes. Measurements were performed with the same volunteer and location on the same day. Data for skin-electrode impedance are reported as mean ± standard deviation (n = 3). (d) Configuration of ECG measurements in a volunteer. Positive (PE) and ground (GE) electrodes positioned on the left forearm and the negative electrode (NE) was placed on the right forearm.

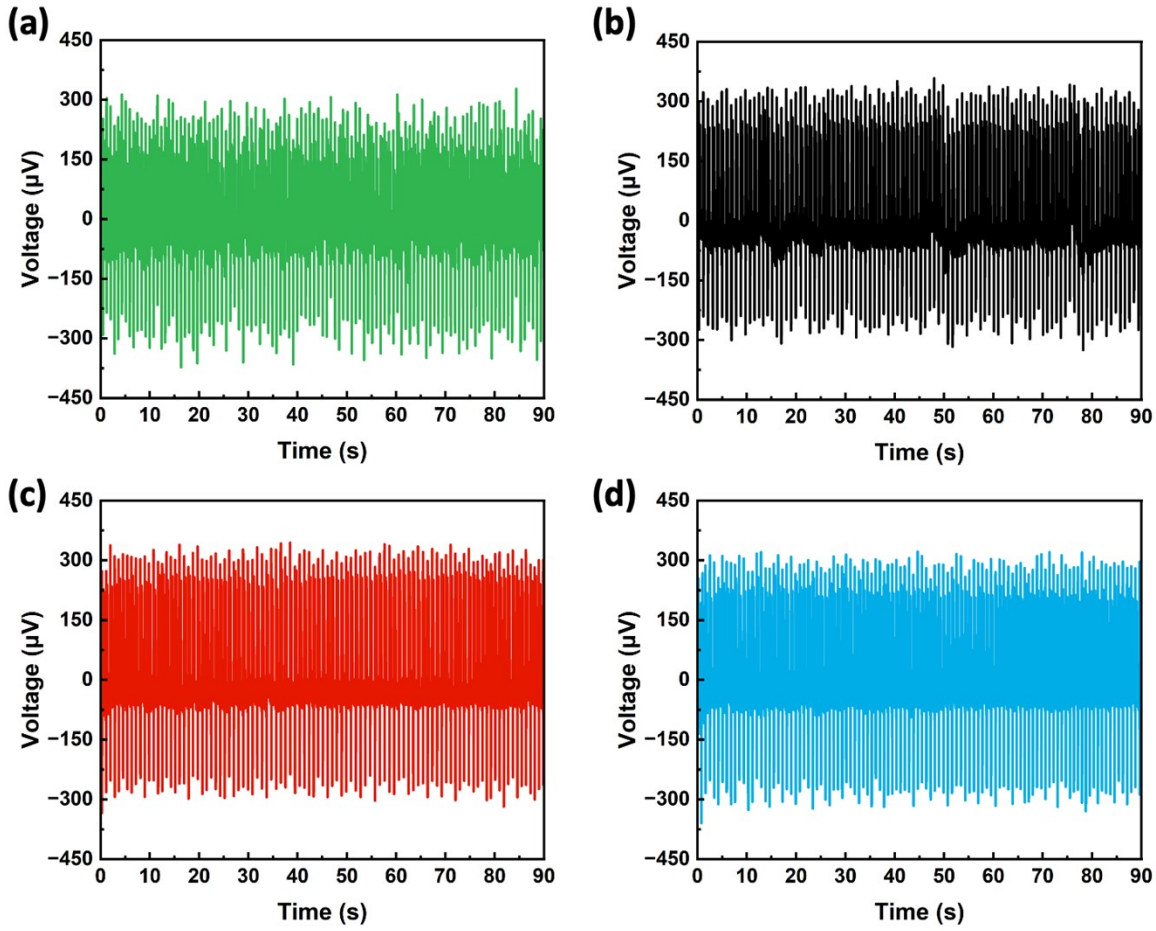

Figure S11. ECG signal recording for 90 s with using commercial (a) PEDOT:PSS/PU/PEG film electrodes before (green) and (b) after self-healing (black) and (c) recycling (red) and (d) Natus® Ag/AgCl gel (blue) electrodes.

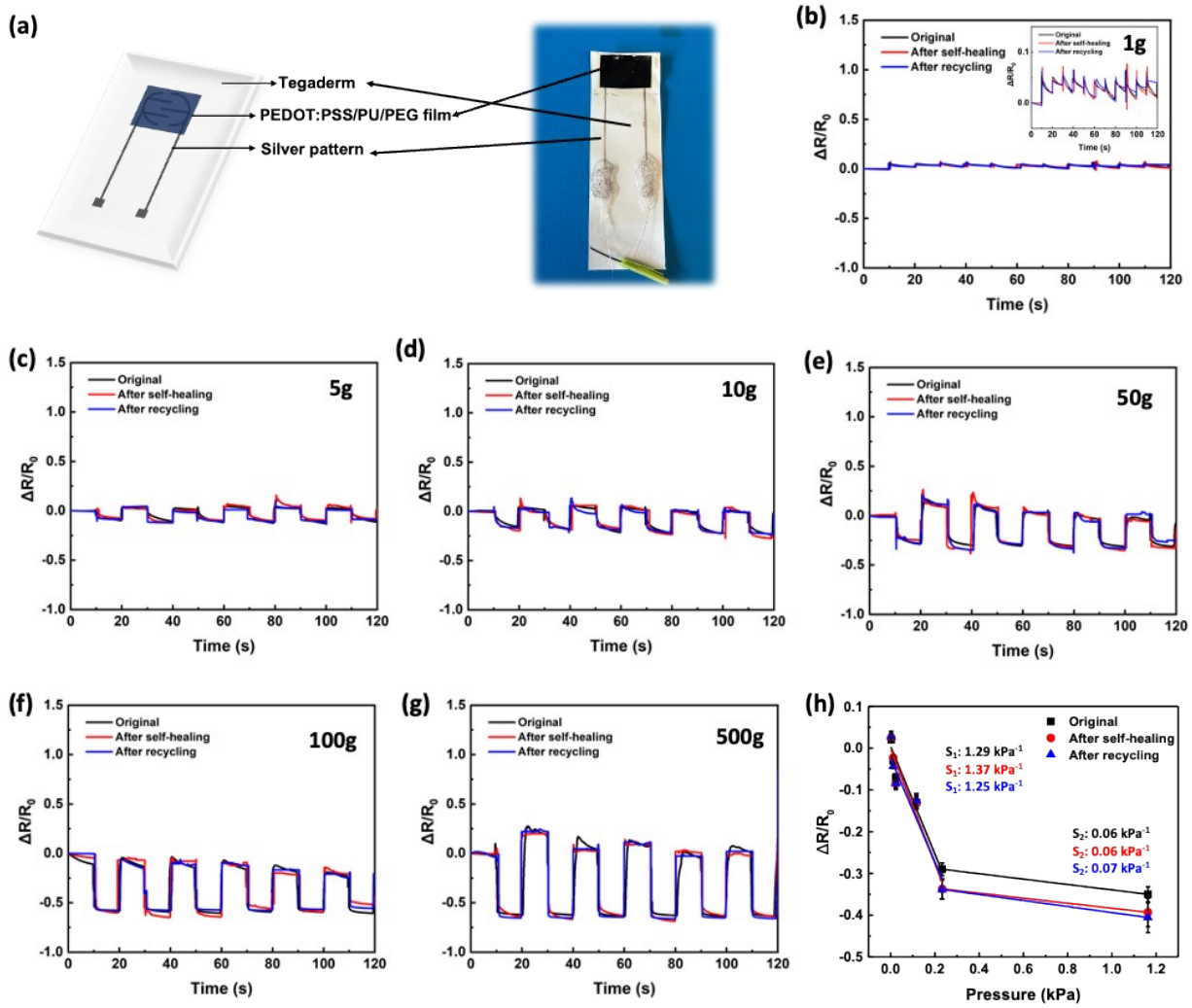

Figure S12. (a) Scheme and photo of resistive pressure sensor based on PEDOT:PSS/PU/PEG film (3rd layer) with printed Ag pattern contact (2nd layer) on Tegaderm substrate (1st layer). Real-time resistance change (ΔR/R0 vs. time) with repeated application of (b) 1 g, (c) 5 g, (d) 10 g, (e) 50 g, (f) 100 g, (g) 500 g weight on the original (black), self-healing (red), and recycled (blue) PEDOT:PSS/PU/PEG films. The same film was used for all the measurements. (h) Sensitivity curves extracted for the original pressure sensor after self-healing and recycling.

The working principle of our pressure sensor is based on the change of contact resistance at the Ag/PEDOT:PSS/PU/PEG interface upon applying pressure. We observed two pressure sensitivity ranges. For an applied pressure up to 0.2 kPa, two mechanisms contribute to the steep contact resistance reduction: i) new electrical connections formed between Ag and PEDOT:PSS/PU/PEG, and ii) the increased

contact area for the existing electrical contacts. For the higher-pressure range, the lower sensitivity suggests that the change of resistance predominantly depends on the increased contact area.

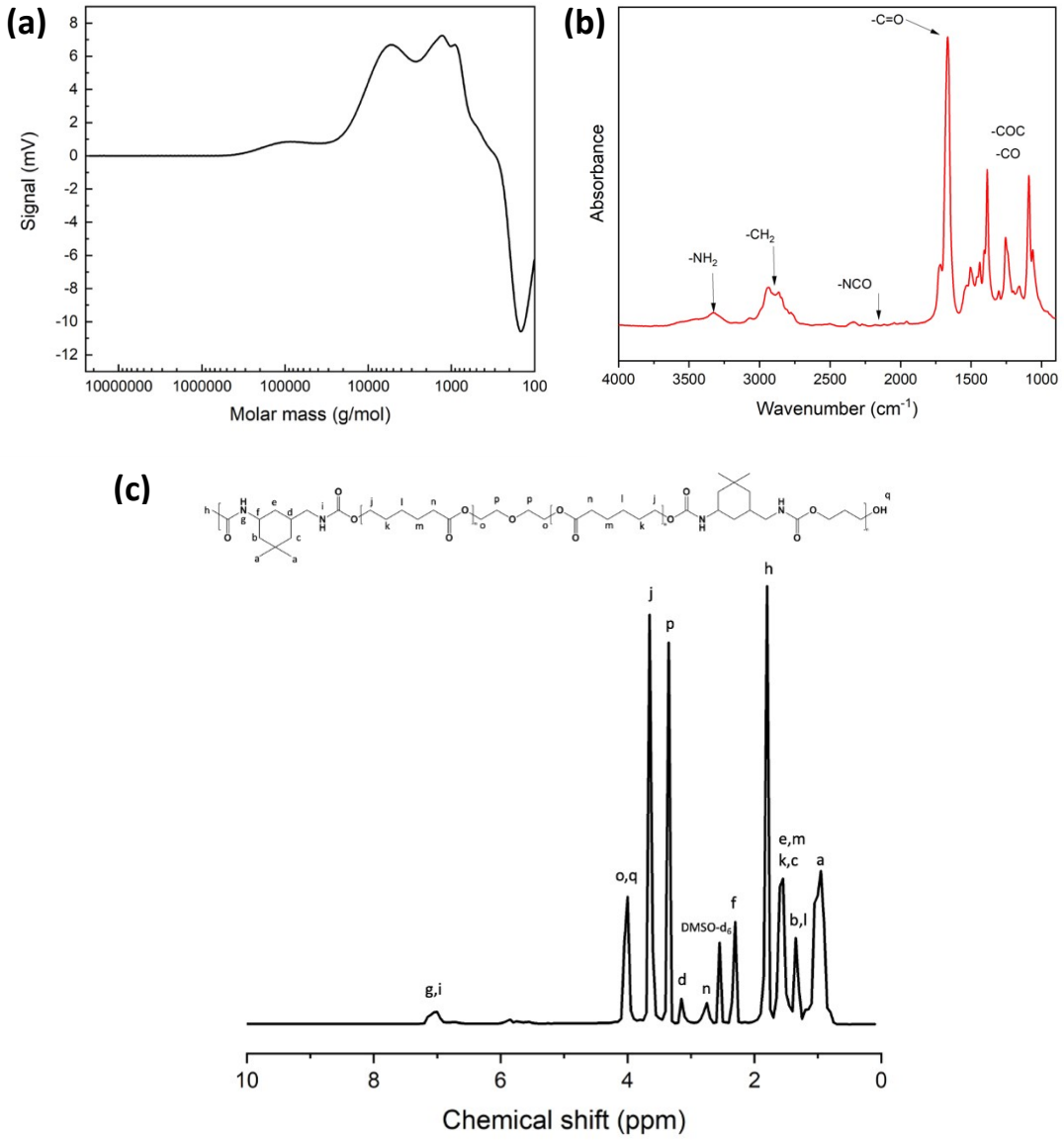

Figure S13. (a) GPC, (b) FTIR and (c) H^1NMR spectra of the self-healing polyurethane synthesized for this work.

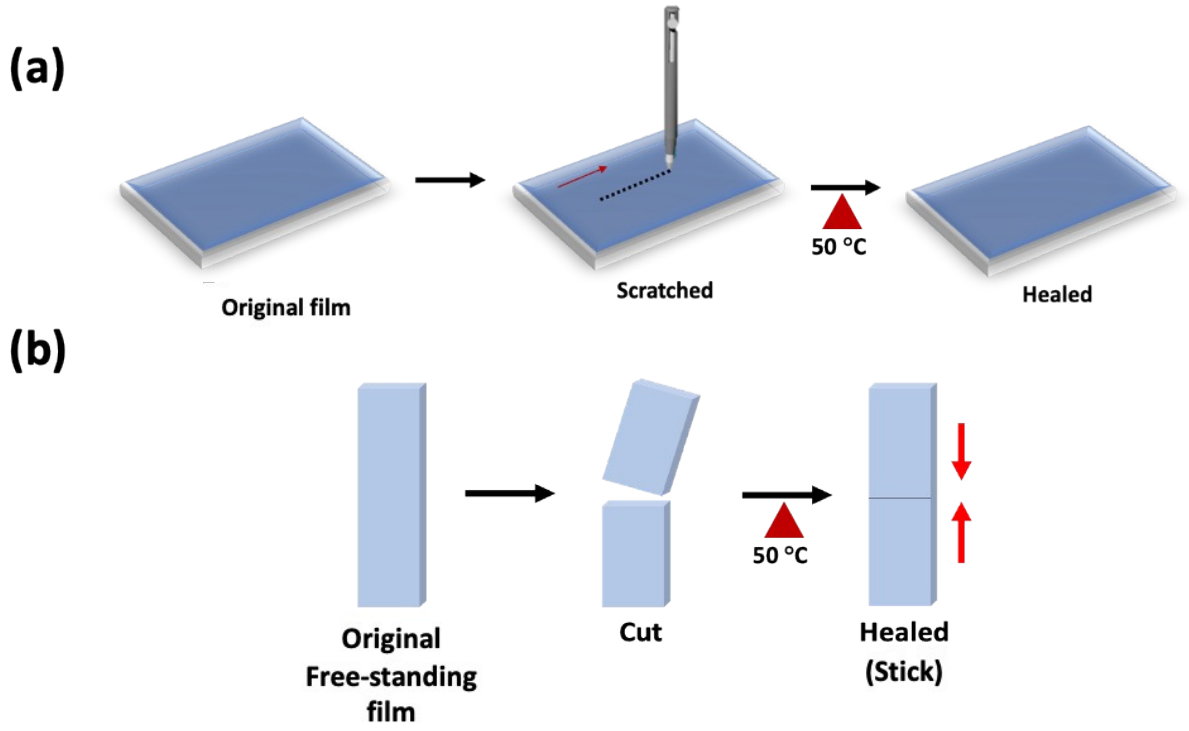

Figure S14. Demonstration of mechanical self-healing experiments used in this study: (a) scratch test and (b) cut-stick test.

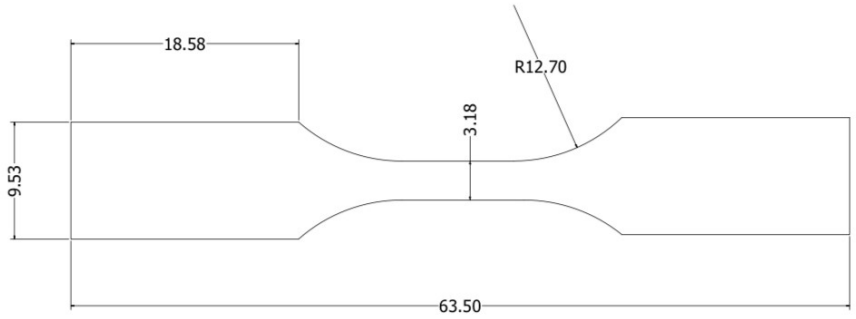

Figure S15. Dog bone mold of ASTM D638 type V

References

1. Y. Li, X. Li, S. Zhang, L. Liu, N. Hamad, S. R. Bobbara, D. Pasini and F. Cicoira, *Advanced Functional Materials*, 2020, **30**, 2002853.
2. J. Y. Oh, S. Kim, H. K. Baik and U. Jeong, *Advanced Materials*, 2016, **28**, 4455-4461.
3. S. Zhang and F. Cicoira, *Advanced Materials*, 2017, **29**, 1703098.
4. L. V. Kayser, M. D. Russell, D. Rodriquez, S. N. Abuhamdieh, C. Dhong, S. Khan, A. N. Stein, J. Ramírez and D. J. Lipomi, *Chem Mater*, 2018, **30**, 4459-4468.
5. X. Q. Su, X. H. Wu, S. Chen, A. M. Nedumaran, M. Stephen, K. Q. Hou, B. Czarny and W. L. Leong, *Advanced Materials*, 2022, **34**, 2200682.
6. T. Wang, Y. Zhang, Q. C. Liu, W. Cheng, X. R. Wang, L. J. Pan, B. X. Xu and H. X. Xu, *Advanced Functional Materials*, 2018, **28,** 1705551.
7. Y. Li, S. M. Zhang, N. Hamad, K. Kim, L. Liu, M. Lerond and F. Cicoira, *Macromol Biosci*, 2020, **20**, 2000146.
8. Y. Lu, Z. Q. Liu, H. M. Yan, Q. Peng, R. G. Wang, M. E. Barkey, J. W. Jeon and E. K. Wujcik, *Acs Applied Materials & Interfaces*, 2019, **11**, 20453-20464.
9. F. Y. Sun, Z. X. Li, S. L. Gao, Y. Y. He, J. C. Luo, X. Zhao, D. D. Yang, T. Gao, H. B. Yang and P. F. Cao, *Acs Applied Materials & Interfaces*, 2022, **14**, 26014-26023.
10. R. Li, T. Fan, G. X. Chen, H. J. Xie, B. Su and M. H. He, *Chem Eng J*, 2020, **393**, 124595.